Turbo-detected unequal protection MPEG-4 wireless video telephony using multi-level coding, trellis coded modulation and space-time trellis coding

S.X. Ng, J.Y. Chung and L. Hanzo

Abstract: Most multimedia source signals are capable of tolerating lossy, rather than lossless delivery to the human eye, ear and other human sensors. The corresponding lossy and preferably low-delay multimedia source codecs however exhibit unequal error sensitivity, which is not the case for Shannon's ideal entropy codec. This paper proposes a jointly optimised turbo transceiver design capable of providing unequal error protection for MPEG-4 coding aided wireless video telephony. The transceiver investigated consists of space-time trellis coding (STTC) invoked for the sake of mitigating the effects of fading, in addition to bandwidth efficient trellis coded modulation or bit-interleaved coded modulation, combined with a multi-level coding scheme employing either two different-rate non-systematic convolutional codes (NSCs) or two recursive systematic convolutional codes for yielding a twin-class unequal-protection. A single-class protection based benchmark scheme combining STTC and NSC is used for comparison with the unequal-protection scheme advocated. The video performance of the various schemes is evaluated when communicating over uncorrelated Rayleigh fading channels. It was found that the proposed scheme requires about 2.8 dBs lower transmit power than the benchmark scheme in the context of the MPEG-4 videophone transceiver at a similar decoding complexity.

1 Motivation and background

Trellis coded modulation (TCM) [1, 2] constitutes a bandwidth-efficient joint channel coding and modulation scheme, which was originally designed for transmission over additive white Gaussian noise (AWGN) channels. By contrast, bit-interleaved coded modulation (BICM) [3] employing parallel bit-based interleavers was designed for communicating over uncorrelated Rayleigh fading channels. Therefore, TCM outperforms BICM, when communicating over AWGN channels since TCM exhibits a higher Euclidean distance. By contrast, the opposite is true, when communicating over uncorrelated Rayleigh fading channels, since BICM exhibits a higher Hamming distance. Space-time trellis coding (STTC) schemes [4, 5], which employ multiple transmit and receive antennas are capable of providing both spatial diversity gain and coding gain. Note that when the spatial diversity order is sufficiently high, the channel's Rayleigh fading envelope is transformed to a Gaussian-like near-constant envelope. Hence, the benefits of a TCM scheme designed for AWGN channels will be efficiently exploited, when TCM is concatenated with STTC in comparison to BICM [6].

Multi-level coding (MLC) schemes [7] have been widely designed for providing unequal error protection capabilities [8]. In this paper, we design a twin-class unequal protection MLC scheme by employing two different code-rate maximal minimum distance non-systematic convolutional codes (NSCs) [9] or recursive systematic convolutional codes (RSCs) [1, 2] as the constituent codes. More specifically, a stronger NSC/RSC is used for protecting the more sensitive video bits, while a weaker NSC/RSC is employed for protecting the less sensitive video bits. Note that TCM employs a set partitioning (SP) based bit mapper [1], where the signal set is split into a number of subsets, such that the minimum Euclidean distance of the signal points in the new subset is increased at every partitioning step. Hence, the NSC/RSC encoded bits which are based on the more sensitive video bits are also mapped to the constellation subsets having the highest minimum Euclidean distance for the sake of further enhanced protection. The TCM and STTC encoders may be viewed as a 'coded mapper' for the unequal protected MLC scheme.

The MPEG-4 standard [10, 11] offers a framework for a whole range of multimedia applications, such as teleshopping, interactive TV, Internet games or iterative mobile video telephony. The novel contribution of this paper is that the state-of-the-art MPEG-4 video codec was amalgamated with a systematically designed sophisticated turbo transceiver using MLC for providing unequal error protection, TCM for maintaining bandwidth efficiency and STTC for attaining spatial diversity. Extrinsic information was exchanged across three serially concatenated decoder stages and the decoding convergence was studied using novel three-dimensional (3-D) non-binary extrinsic information transfer (EXIT) charts [12]. We will refer to this unequal-protection joint MPEG-4 source-coding, channel-coding, modulation and spatial diversity aided turbo-transceiver as the STTC-TCM-2NSC or STTC-TCM-2RSC scheme. We will also investigate the STTC-BICM-2RSC scheme, where

IEE Proceedings online no. 20050236

doi:10.1049/ip-com:20050236

Paper first received 23rd May 2005 and in final revised form 9th June 2005

The authors are with the School of Electronics and Computer Science, University of Southampton, SO17 1BJ, UK

E-mail: sxn@ecs.soton.ac.uk

BICM is employed as the inner code for the sake of studying the performance difference between BICM and TCM as the inner code in the STTC-based unequal-protection turbo transceiver, it is shown that significant iteration gains are attained with the aid of an efficient iterative decoding mechanism.

2 The turbo transceiver

The schematic of the serially concatenated STTC-TCM/BICM-2NSC/2RSC turbo scheme using a STTC, a TCM/BICM and two NSCs/RSCs as its constituent codes is depicted in Fig. 1. The MPEG-4 codec operated at $R_f = 30$ frames per second using the (176×144)-pixel quarter common intermediate format (QCIF) Miss America video sequence, encoded at a near-constant bitrate of $R_b = 69$ kbit/s. Hence, we have $R_b/R_f = 2300$ bits per video frame. We partition the video bits into two unequal-protection classes. Specifically, class-1 and class-2 consist of 25% (which is 575 bits) and 75% (which is 1725 bits) of the total number of video bits, respectively. The more sensitive video bits constituted mainly by the MPEG-4 framing and synchronisation bits are in class-1 and they are protected by a stronger binary NSC/RSC having a coding rate of $R_1 = k_1/n_1 = 1/2$ and a code memory of $L_1 = 3$. The less sensitive video bits – predominantly signalling the MPEG-4 discrete cosine transform (DCT) coefficients and motion vectors – are in class-2 and they are protected by a weaker non-binary NSC/RSC having a coding rate of $R_2 = k_2/n_2 = 3/4$ and a code memory of $L_2 = 3$. Hence, the effective code rate for the MLC scheme employing the $R_1 = 1/2$ and $R_2 = 3/4$ NSCs/RSCs is given by $R_{MLC} = (k_1 + k_2)/(n_1 + n_2) = 2/3$. Note that the number of MPEG-4 framing and synchronisation bits is only about 10% of the total number of video bits. Hence, about $25\% - 10\% = 15\%$ of the class-1 bits are constituted by the video bits signalling the most sensitive MPEG-4 DCT coefficients. We invoke code termination bits in both NSCs/RSCs and hence the number of coded bits emerging from the $R_1 = 1/2$ binary NSC/RSC encoder is $(575 + k_1 L_1)/R_1 = 1156$ bits, while that generated by the $R_2 = 3/4$ non-binary NSC/RSC encoder is $(1725 + k_2 L_2)/R_1 = 2312$ bits.

The class-1 and class-2 NSC/RSC coded bit sequences seen in Fig. 1 are interleaved by two separate bit interleavers of length 1156 and 2312 bits, respectively. The two interleaved bit sequences are then concatenated to form a bit sequence of $1156 + 2312 = 3468$ bits. This bit sequence is then fed to the TCM/BICM encoder of Fig. 1 having a coding rate of $R_3 = k_3/n_3 = 3/4$ and a code memory of $L_4 = 3$. When the SP-based TCM is employed, the most significant bit (MSB) of the three-bit input symbol in the rate-3/4 TCM encoder has a higher protection. Therefore, we map the interleaved bit sequence of the class-1 NSC/RSC encoder to the MSB of the TCM scheme's three-bit input symbol for the sake of further protecting the class-1 video bits. Hence, the MLC encoder of Fig. 1, which consists of two NSC/RSC encoders, can be viewed as a non-binary outer encoder providing 3-bit MLC symbols, denoted as $\mathbf{u}$ in Fig. 1, for the rate-3/4 TCM/BICM encoder. We employ code termination also in the TCM/BICM scheme and hence at the TCM/BICM encoder's output we have $(3468 + k_3 L_3)/R_3 = 4636$ bits or $4636/4 = 1159$ symbols. The TCM symbol sequence (or BICM bit sequence) is then symbol-interleaved (or bit-interleaved) in Fig. 1 and fed to the STTC encoder. We invoke a 16-state STTC scheme having a code memory of $L_4 = 4$ and $N_t = 2$ transmit antennas, employing $M = 16$-level quadrature amplitude modulation (16 QAM). We terminate the STTC code by a 4-bit 16 QAM symbol, since we have $N_t = 2$. Therefore, at each transmit antenna we have $1159 + 1 = 1160$ 16 QAM symbols or $4 \times 1160 = 4640$ bits in a transmission frame. The overall coding rate is given by $R = 2300/4640 = 0.496$ and the effective throughput of the system is $\log_2(M)R = 1.98$ bits per symbol (BPS). The STTC decoder employed $N_r = 2$ receive antennas and the received signals are fed to the iterative decoders for the sake of estimating the video bit sequences in both class-1 and class-2, as seen in Fig. 1.

2.1 The turbo decoding

The STTC-TCM-2RSC scheme's turbo decoder structure is illustrated in Fig. 2, where there are four constituent decoders, each labelled with a round-bracketed index. Symbol-based and bit-based MAP algorithms [2] operating in the logarithmic-domain are employed by the TCM in addtion to the rate $R_2 = 3/4$ RSC decoders and by the $R_1 = 1/2$ RSC decoder, respectively. The notations $P(\cdot)$ and $L(\cdot)$ in Fig. 2 denote the logarithmic-domain symbol probabilities and the logarithmic-likelihood ratio (LLR) of the bit probabilities, respectively. The notations c, u and b_i in the round brackets $(\cdot)$ in Fig. 2 denote TCM coded symbols, TCM information symbols and the class-i video bits, respectively. The specific nature of the probabilities and LLRs is represented by the subscripts *a, p, e* and *i*, which denote in Fig. 2 *a priori*, *a posteriori*, extrinsic, and intrinsic information, respectively. The probabilities and LLRs associated with one of the four constituent decoders having a label of $\{1, 2, 3a, 3b\}$ are differentiated by the identical superscripts of $\{1, 2, 3a, 3b\}$. Note that the superscript 3 is used for representing the MLC decoder of Fig. 2 which invokes the RSC decoders of 3*a* and 3*b*.

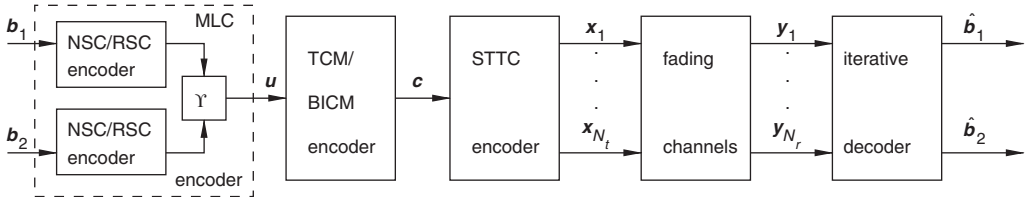

Fig. 1 *Block diagram of the serially concatenated STTC-TCM/BICM-2NSC/2RSC scheme*

The notations $\boldsymbol{b}_i$, $\hat{\boldsymbol{b}}_i$, $\boldsymbol{u}$, $\boldsymbol{c}$, $\boldsymbol{x}_j$ and $\boldsymbol{y}_k$ denote the vectors of the class-i video bits, the estimates of the class-i video bits, the MLC coded symbols, the TCM coded symbols (or BICM coded bits), the STTC coded symbols for transmitter j and the received symbols at receiver k, respectively. Furthermore, Υ is a bit-to-symbol converter, while N_t and N_r denote the number of transmitters and receivers, respectively. The symbol-based (or bit-based) channel interleaver between the STTC and TCM (or BICM) schemes in addition to the two bit-based interleavers at the output of NSC/RSC encoders are not shown for simplicity. The iterative decoder seen at the right is detailed in Fig. 2

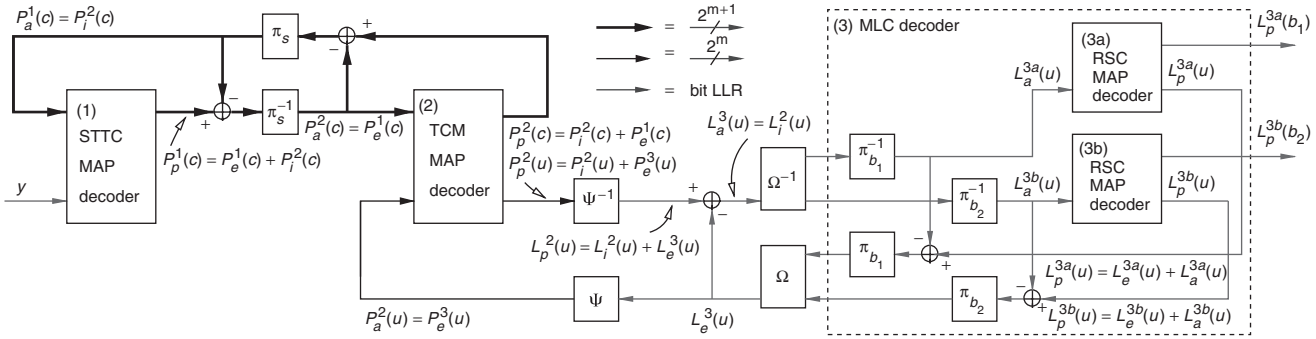

Fig. 2 *Block diagram of the STTC-TCM-2RSC turbo detection scheme*
The notations $\pi_{(s,b_i)}$ and $\pi^{-1}_{(s,b_i)}$ denote the interleaver and deinterleaver, while the subscript s denotes the symbol-based interleaver of TCM and the subscript b_i denotes the bit-based interleaver for class-i RSC. Furthermore, Ψ and Ψ^{-1} denote LLR-to-symbol probability and symbol probability-to-LLR conversion, while Ω and Ω^{-1} denote the parallel-to-serial and serial-to-parallel converter, respectively. The notation m denotes the number of information bits per TCM coded symbol. The thickness of the connecting lines indicates the number of non-binary symbol probabilities spanning from a single LLR per bit to 2^m and 2^{m+1} probabilities

As we can observe from Fig. 2, the STTC decoder of block (1) benefits from the *a priori* information provided by the TCM decoder of block (2), namely from $P_a^1(c) = P_i^2(c)$ regarding the 2^{m+1}-ary TCM coded symbols, where m is the number of information bits per TCM coded symbol. More specifically, $P_i^2(c)$ is referred to here as the intrinsic probability of the 2^{m+1}-ary TCM coded symbols, because it contains the inseparable extrinsic information provided by the TCM decoder itself as well as the *a priori* information regarding the uncoded 2^m-ary TCM input information symbols emerging from the RSC decoders of block (3), namely $P_a^2(u) = P_e^3(u)$. Hence, the STTC decoder indirectly also benefits from the *a priori* information $P_a^2(u) = P_e^3(u)$ provided by the RSC decoders of block (3), potentially enhanced by the TCM decoder of block (2). Similarly, the intrinsic probability of $P_i^2(u)$ provided by the TCM decoder for the sake of the RSC decoders' benefit consists of the inseparable extrinsic information generated by the TCM decoder itself in addition to the systematic information of the STTC decoder, namely $P_a^2(c) = P_e^1(c)$. Note that after the symbol probability-to-LLR conversion, $P_i^2(u)$ becomes $L_i^2(u)$. Therefore, the RSC decoders of block (3) benefit directly from the *a priori* information provided by the TCM decoder of block (2), namely from $L_a^3(u) = L_i^2(u)$ and indirectly from the *a priori* information provided by the STTC decoder of block (1), namely from $P_a^2(c) = P_e^1(c)$. Alternatively, the TCM decoder benefits directly from the STTC and RSC decoders through the *a priori* information of $P_a^2(c) = P_e^1(c)$ and $P_a^2(u) = P_e^3(u)$, respectively, as shown in Fig. 2.

2.2 The turbo benchmark scheme

For the sake of benchmarking the scheme advocated, we created a powerful benchmark scheme by replacing the TCM/BICM and NSC/RSC encoders of Fig. 1 by a single NSC codec having a coding rate of $R_0 = k_0/n_0 = 1/2$ and a code memory of $L_0 = 6$. We will refer to this benchmark scheme as the STTC-NSC arrangement. All video bits are equally protected in the benchmark scheme by a single NSC encoder and a STTC encoder. A bit-based channel interleaver is inserted between the NSC encoder and STTC encoder. Taking into account the bits required for code termination, the number of output bits of the NSC encoder is $(2300 + k_0 L_0)/R_0 = 4612$, which corresponds to 1153 16 QAM symbols. Again, a 16-state STTC scheme having $N_t = 2$ transmit antennas is employed. After code termination, we have $1153 + 1 = 1154$ 16 QAM symbols or $4(1154) = 4616$ bits in a transmission frame at each transmit antenna. Similar to the STTC-TCM/BICM-2NSC/2RSC scheme, the overall coding rate is given by $R = 2300/4616 = 0.498$ and the effective throughput is $\log_2(16)R = 1.99$ BPS, both of which are close to the corresponding values of the proposed scheme.

Let us define a single decoding iteration for the proposed STTC-TCM/BICM-2NSC/2RSC scheme as a combination of a STTC decoding, a TCM/BICM decoding, a class-1 NSC/RSC decoding and a class-2 NSC/RSC decoding step. Similarly, a decoding iteration of the STTC-NSC benchmark scheme is comprised of a STTC decoding and a NSC decoding step. We will quantify the decoding complexity of the proposed STTC-TCM/BICM-2NSC/2RSC scheme and that of the benchmark scheme using the number of decoding trellis states. The total number of decoding trellis states per iteration of the proposed scheme employing 2 NSC/RSC decoders having a code memory of $L_1 = L_2 = 3$, TCM/BICM having $L_3 = 3$ and STTC having $L_4 = 4$, is $S = 2^{L_1} + 2^{L_2} + 2^{L_3} + 2^{L_4} = 40$. By contrast, the total number of decoding trellis states per iteration for the benchmark scheme having a code memory of $L_0 = 6$ and STTC having $L_4 = 4$, is given by $S = 2^{L_0} + 2^{L_4} = 80$. Therefore, the complexity of the STTC-TCM-2NSC/2RSC scheme having two iterations is equivalent to that of the benchmark scheme having a single iteration, which corresponds to 80 decoding states.

3 MIMO channel capacity

Let us consider a multi-input multi-output (MIMO) system employing N_t transmit antennas and N_r transmit antennas. When two-dimensional L-ary PSK/QAM is employed at each transmit antenna, the received signal vector of the MIMO system is given by

$$\boldsymbol{y} = \boldsymbol{H}\boldsymbol{x} + \boldsymbol{n} \tag{1}$$

where $\boldsymbol{y} = (y_1, \ldots, y_{N_r})^T$ is an N_r-element vector of the received signals, $\boldsymbol{H}$ is an $(N_r \times N_t)$-dimensional channel matrix, $\boldsymbol{x} = (x_1, \ldots, x_{N_t})^T$ is an N_t-element vector of the transmitted signals and $\boldsymbol{n} = (n_1, \ldots, n_{N_r})^T$ is an N_r-element noise vector, where each elements in $\boldsymbol{n}$ is an AWGN process

having a zero mean and a variance of $N_0/2$ per dimension. Note that in a MIMO system there are $M = L^{N_t}$ number of possible L-ary PSK/QAM phasor combinations in the transmitted signal vector $\boldsymbol{x}$. The STTC scheme of [4] designed for attaining transmit diversity may in fact be viewed as a rate-$1/N_t$ channel code, where there are only L^1 legitimate space-time codewords out of the L^{N_t} possible phasor combinations during each transmission period. By contrast, Bell Lab's layered space-time (BLAST) scheme [13] designed for attaining multiplexing gain may be viewed as a rate-1 channel code, where all L^{N_t} phasor combinations are legitimate during each transmission period. Despite having different code rates, both the STTC and BLAST schemes have the same channel capacity.

The conditional probability of receiving a signal vector $\boldsymbol{y}$ given that an $M = L^{N_t}$-ary signal vector $\boldsymbol{x}_m$, $m \in \{1, \ldots, M\}$, was transmitted over Rayleigh fading channels is determined by the probability density function (PDF) of the noise, yielding

$$p(\boldsymbol{y}|\boldsymbol{x}_m) = \frac{1}{\pi N_0} \exp\left(\frac{-||\boldsymbol{y} - \boldsymbol{H}\boldsymbol{x}_m||^2}{N_0}\right) \tag{2}$$

In the context of discrete-amplitude QAM [14] and PSK [15] signals, we encounter a discrete-input continuous-output memoryless channel (DCMC) [15]. We derived the channel capacity for a MIMO system, which uses two-dimensional M-ary signalling over the DCMC, from that of the discrete memoryless channel (DMC) [16] as

$$C_{\mathrm{DCMC}} = \max_{p(\boldsymbol{x}_1)\ldots p(\boldsymbol{x}_M)} \sum_{m=1}^{M} \int_{-\infty}^{\infty} p(\boldsymbol{y}|\boldsymbol{x}_m)\, p(\boldsymbol{x}_m) \times \log_2\left(\frac{p(\boldsymbol{y}|\boldsymbol{x}_m)}{\sum_{n=1}^{M} p(\boldsymbol{y}|\boldsymbol{x}_n)\, p(\boldsymbol{x}_n)}\right) d\boldsymbol{y} \ [\mathrm{bit/sym}] \tag{3}$$

where $p(\boldsymbol{x}_m)$ is the probability of occurrence for the transmitted signal vector $\boldsymbol{x}_m$. It was shown in [16] that for a symmetric DMC, the full capacity may only be achieved by using equiprobable inputs. Hence, the right hand side of (3), which represents the mutual information between $\boldsymbol{x}$ and $\boldsymbol{y}$, is maximised, when the transmitted symbols are equiprobably distributed, i.e. when we have $p(\boldsymbol{x}_m) = 1/M$ for $m \in \{1, \ldots, M\}$. Hence, by using $p(\boldsymbol{x}_m) = 1/M$ and after a range of mathematical manipulations, (3) can be simplified to

$$C_{\mathrm{DCMC}} = \log_2(M) - \left(\frac{1}{M}\right) \sum_{m=1}^{M} E\left[\log_2 \sum_{n=1}^{M} \exp(\Phi_{m,n}) \middle| \boldsymbol{x}_m\right] \ [\mathrm{bit/sym}] \tag{4}$$

where $E[f(\boldsymbol{y}|\boldsymbol{x}_m)|\boldsymbol{x}_m] = \int_{-\infty}^{\infty} f(\boldsymbol{y}|\boldsymbol{x}_m)\, p(\boldsymbol{y}|\boldsymbol{x}_m) d\boldsymbol{y}$ is the expectation of the function $f(\boldsymbol{y}|\boldsymbol{x}_m)$ conditioned on $\boldsymbol{x}_m$. The expectation in (4) is taken over $\boldsymbol{H}$ and $\boldsymbol{n}$, while $\Phi_{m,n}$ is given by

$$\Phi_{m,n} = \frac{-||\boldsymbol{H}(\boldsymbol{x}_m - \boldsymbol{x}_n) + \boldsymbol{n}||^2 + ||\boldsymbol{n}||^2}{N_0} = \sum_{i=1}^{N_r} \frac{-|\boldsymbol{h}_i(\boldsymbol{x}_m - \boldsymbol{x}_n) + \boldsymbol{n}_i|^2 + |\boldsymbol{n}_i|^2}{N_0} \tag{5}$$

where $\boldsymbol{h}_i$ is the ith row of $\boldsymbol{H}$ and $\boldsymbol{n}_i$ is the AWGN at the ith receiver.

When the channel input is a continuous-amplitude, discrete-time Gaussian-distributed signal, we encounter a continuous-input continuous-output memoryless channel (CCMC) [15], where the capacity is only restricted either by the signalling energy or by the bandwidth. It was shown in [17, 18] that the MIMO capacity of the CCMC can be expressed as

$$C_{\mathrm{CCMC}} = E\left[WT \sum_{i=1}^{r} \log_2\left(1 + \lambda_i \frac{SNR}{N_t}\right)\right] \tag{6}$$

where W is the bandwidth and T is the signalling period of the finite-energy signalling waveform and r is the rank of $\boldsymbol{Q}$, which is defined as $\boldsymbol{Q} = \boldsymbol{H}^H\boldsymbol{H}$ for $N_r \geq N_t$ or $\boldsymbol{Q} = \boldsymbol{H}\boldsymbol{H}^H$ for $N_r < N_t$. Furthermore, λ_i is the ith eigenvalue of the matrix $\boldsymbol{Q}$.

However, for the special case of an orthogonal MIMO transmission system, such as the orthogonal space time block coding (STBC) scheme of [19, 20], the received signal in (1) can be transformed into [21]

$$y_i = \sum_{j=1}^{N_t} |h_{i,j}|^2 x + \Omega_i = \chi^2_{2N_t,i} x + \Omega_i, \quad i = \{1, \ldots, N_r\} \tag{7}$$

where y_i is the received signal at receiver i in the received signal vector $\boldsymbol{y}$ and x is the complex-valued (two-dimensional) transmitted signal, $h_{i,j}$ is the complex-valued Rayleigh fading coefficient between transmitter j and receiver i, $\chi^2_{2N_t,i} = \sum_{j=1}^{N_t} |h_{i,j}|^2$ represents a chi-squared distributed random variable having $2N_t$ degree of freedom at receiver i and Ω_i is the ith receiver's complex-valued AWGN after transformation, which has a zero mean and a variance of $\chi^2_{2N_t,i} N_0/2$ per dimension. Owing to orthogonal transmissions, the MIMO channel was transformed into a single-input multi-output (SIMO) channel, where the equivalent Rayleigh fading coefficient between the transmitter and the ith receiver is given by $\chi^2_{2N_t,i}$ and the equivalent noise at the ith receiver is given by Ω_i. Since the MIMO channel has now been transformed into a SIMO channel, we have $M = L^1 = L$, since there is only a single transmit antenna in a SIMO scheme. The channel capacity of STBC can be shown to be

$$C^{\mathrm{STBC}}_{\mathrm{DCMC}} = \log_2(M) - \frac{1}{M} \times \sum_{m=1}^{M} E\left[\log_2 \sum_{n=1}^{M} \exp(\Phi^{\mathrm{STBC}}_{m,n}) \middle| x_m\right] \ [\mathrm{bit/sym}] \tag{8}$$

where the expectation in (8) is taken over $\chi^2_{2N_t,i}$ and Ω_i, while $\Phi^{\mathrm{STBC}}_{m,n}$ is given by

$$\Phi^{\mathrm{STBC}}_{m,n} = \sum_{i=1}^{N_r} \frac{-\left|\chi^2_{2N_t,i}(x_m - x_n) + \Omega_i\right|^2 + |\Omega_i|^2}{\chi^2_{2N_t,i} N_0} \tag{9}$$

Furthermore, the CCMC capacity for STBC can be shown to be

$$C^{\mathrm{STBC}}_{\mathrm{CCMC}} = E\left[WT \log_2\left(1 + \sum_{i=1}^{N_r} \chi^2_{2N_t,i} \frac{SNR}{N_t}\right)\right] \ [\mathrm{bit/sym}] \tag{10}$$

Figure 3 shows the MIMO channel capacity limit of STTC and STBC schemes employing 16 QAM and $N_t = N_r = 2$. As we can see from Fig. 3, the channel capacity of STBC is lower than that of STTC owing to employing orthogonal transmissions. Note that STBC achieves only diversity gain but no coding gain. However, the coding gain of STTC is achieved at the cost of a higher

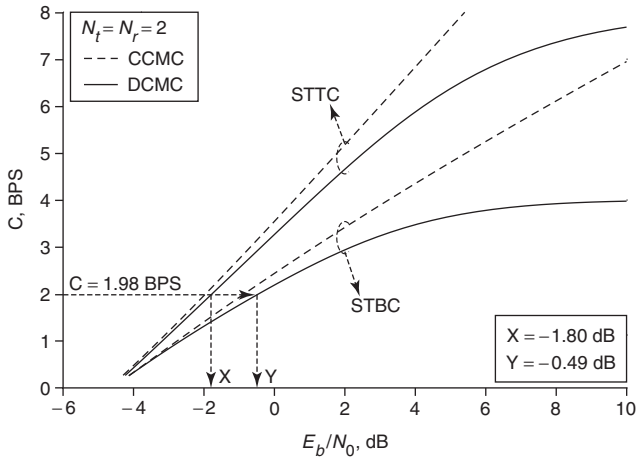

Fig. 3 *The MIMO channel capacity limit for STTC and STBC schemes employing 16QAM and $N_t = N_r = 2$*

trellis-based decoding complexity. The MIMO channel capacity limit of STTC determined from (4) at a throughput of 1.98 BPS and 1.99 BPS is $E_b/N_0 = -1.80$ dB and -1.79 dB, respectively. The corresponding channel capacity limit of STBC evaluated from (8) is $E_b/N_0 = -0.49$ dB and -0.47 dB, respectively.

4 Convergence analysis

EXIT charts [22] have been widely used for analysing the convergence behaviour of iterative decoding aided concatenated coding schemes. A specific novelty of this paper is that we will employ the technique proposed in [12] for computing the non-binary EXIT functions, where the multidimensional histogram computation of [23, 24] is replaced by the lower-complexity averaging of the extrinsic symbol probabilities of the MAP decoders. Let us study the convergence of the proposed three-component STTC-TCM-2RSC scheme using 3-D EXIT charts [25], when communicating over MIMO Rayleigh fading channels. As we can see from Fig. 2, the TCM decoder receives inputs from and provides outputs for both the STTC and the MLC decoders of Fig. 2. Hence, we have to compute two EXIT planes, the first one corresponding to the TCM decoder's intrinsic probabilities $P_i^2(c)$ provided for the STTC decoder and the second one corresponding to $P_i^2(u)$ supplied for the MLC decoders, as shown in Fig. 2. By contrast, the STTC decoder has a single EXIT plane characterising its extrinsic probability $P_e^1(c)$ forwarded to the TCM decoder in Fig. 2. Similarly, the MLC decoder has one EXIT plane characterising its extrinsic probability $P_e^3(u)$ forwarded to the TCM decoder in Fig. 2.

Let us denote the average *a priori* information and the average extrinsic (or intrinsic for TCM) information as I_A and I_E, respectively. The I_A (probabilities or LLRs) and I_E (probabilities or LLRs) quantities of TCM corresponding to the links with the STTC and MLC schemes are differentiated by the subscripts 1 and 2, respectively. Similar to computing the conventional EXIT curve in a 2-D EXIT chart, we have to model/provide the *a priori* information I_A for each of the inputs of a constituent decoder in order to compute the EXIT plane of that constituent decoder in a 3-D EXIT chart. When a long bit interleaver is used between two non-binary constituent decoders, I_A can indeed be sufficiently accurately modelled based on the assumption of having independent bits within the non-binary symbol [22]. More explicitly, for the bit-interleaved decoder, I_A can be computed based on the average mutual information obtained, when binary phase shift keying (BPSK) modulated signals are transmitted across AWGN channels. To expound further, since the MLC coded bits are bit-interleaved before feeding them to the TCM encoder, we model both the average *a priori* information provided for the TCM decoder, namely $I_{A2}(\text{TCM}) = f(P_a^2(u))$ corresponding to the non-binary TCM input symbol, as well as the average *a priori* information generated for the MLC decoder, namely $I_A(\text{MLC}) = f(P_i^2(c))$ corresponding to the non-binary MLC coded symbol, where $f(\cdot)$ represents the EXIT function, by assuming that the MLC coded bits in a non-binary MLC coded symbol are independent of each other.

By contrast, the bits in a non-binary coded symbol of a symbol-interleaved concatenated coding scheme are not independent. Hence, for the symbol-interleaved links between the 16 QAM-based TCM and STTC scheme, the distribution of the bits in a non-binary coded symbol cannot be sufficiently accurately modelled using independent BPSK modulation. In this scenario, we found that when the average *a priori* information generated for these 4-bit TCM coded symbols is modelled based on the average mutual information obtained when 16 QAM modulated signals are transmitted across AWGN channels, a good EXIT plane approximation can be obtained. Note that the average mutual information of 16 QAM in AWGN channels is given by the AWGN channel's capacity computed for 16 QAM (i.e. the DCMC capacity [14]) provided that all the 16 QAM symbols are equiprobable. Therefore, the average *a priori* information provided for the TCM decoder, namely $I_{A1}(\text{TCM}) = f(P_a^2(c))$, and the average *a priori* information for STTC decoder, namely $I_A(\text{STTC}) = f(P_a^1(c))$, are generated based on the AWGN channel's capacity determined for 16 QAM.

Figures 4 and 5 illustrate the 3-D EXIT charts and the iteration trajectories for the proposed STTC-TCM-2RSC scheme at $E_b/N_0 = -0.5$ dB, when an interleaver block length of 10 000 16 QAM symbols is employed, where E_b/N_0 is the signal-to-noise ratio (SNR) per information bit.

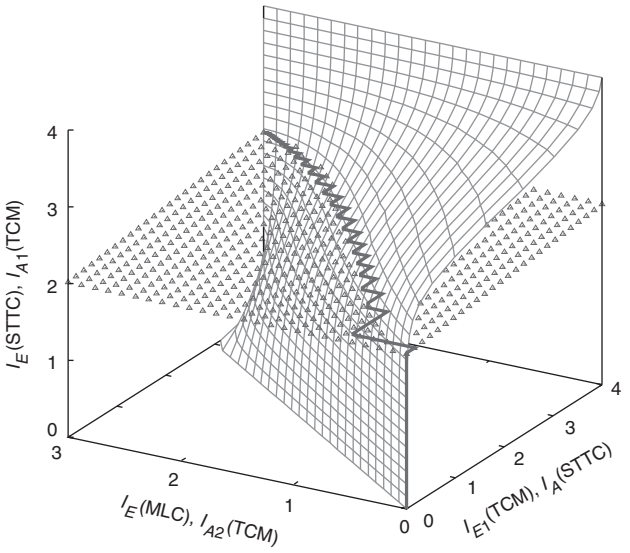

Fig. 4 *The 3-D EXIT chart and the iteration trajectory between the STTC and TCM decoders at $E_b/N_0 = -0.5$ dB, when a block length of 10 000 16QAM symbols is used*
The EXIT plane marked with triangles was computed based on the STTC decoder's output $P_e^1(c)$ and the EXIT plane drawn using lines was computed based on the TCM decoder's output $P_i^2(c)$

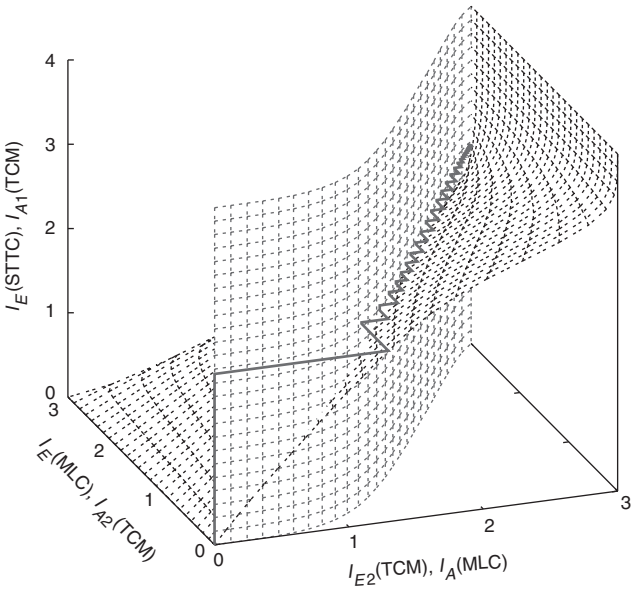

Fig. 5 *The 3-D EXIT chart and the iteration trajectory between the TCM and MLC decoders at $E_b/N_0 = -0.5$ dB, when a block length of 10 000 16QAM symbols is used*
The EXIT plane spanning from the vertical line $[I_E(\text{MLC}) = 0, I_A(\text{MLC}) = 0, I_E(\text{STTC}) = \{0 \rightarrow 4\}]$ to the vertical line $[I_E(\text{MLC}) = 3, I_A(\text{MLC}) = 3, I_E(\text{STTC}) = \{0 \rightarrow 4\}]$ was computed based on the MLC decoder's output $P_e^3(c)$ and the other EXIT plane was computed based on the TCM decoder's output $P_i^2(u)$

Specifically, the EXIT plane marked with triangles in Fig. 4 was computed based on the STTC decoder's output $P_e^1(c)$ at the given I_E(MLC) and I_A(STTC) abscissa values, while the EXIT plane drawn using lines in Fig. 4 was computed based on the TCM decoder's output $P_i^2(c)$ at the given I_{A1}(TCM) and I_{A2}(TCM) value. Similarly, the EXIT plane of Fig. 5 spanning from the vertical line $[I_E(\text{MLC}) = 0, I_A(\text{MLC}) = 0, I_E(\text{STTC}) = \{0 \rightarrow 4\}]$ to the vertical line $[I_E(\text{MLC}) = 3, I_A(\text{MLC}) = 3, I_E(\text{STTC}) = \{0 \rightarrow 4\}]$ was computed based on the MLC decoder's output $P_e^3(c)$ at the given I_E(STTC) and I_A(MLC). The other EXIT plane of Fig. 5 spanning from the horizontal line $[I_{A2}(\text{TCM}) = \{0 \rightarrow 3\}, I_{E2}(\text{TCM}) = 0, I_{A1}(\text{TCM}) = 0]$ to the horizontal line $[I_{A2}(\text{TCM}) = \{0 \rightarrow 3\}, I_{E2}(\text{TCM}) = 3, I_{A1}(\text{TCM}) = 4]$ was computed based on the TCM decoder's output $P_i^2(u)$ at the given I_{A1}(TCM) and I_{A2}(TCM) values.

As we can see from Fig. 4, the iteration trajectory computed based on the average intrinsic information of the TCM decoder's output, namely $I_{E1}(\text{TCM}) = f(P_i^2(c))$, is under the STTC-EXIT plane marked with triangles and above the TCM-EXIT plane drawn using lines. Note that the approximated EXIT-planes in Fig. 4 failed to mimic the exact distribution of the TCM coded symbols, and hence resulted in some overshooting mismatches between the EXIT-planes and the trajectory. However, as seen from Fig. 5, the mismatch between the EXIT-planes and the trajectory computed based on the average intrinsic information of the TCM decoder's output, namely $I_{E2}(\text{TCM}) = f(P_i^2(u))$, is minimal. Explicitly, the trajectory seen in Fig. 5 is located on the right of the MLC-EXIT plane spanning two vertical lines and on the left of the TCM-EXIT plane spanning two horizontal lines. Note from Fig. 5 that I_{E2}(TCM) is not strictly monotonically increasing with I_E(STTC), which is in contrast to the bit-interleaved system of [25]. Hence, we cannot combine Figs. 4 and 5 into a single 3-D EXIT chart, as it is in [25].

As we can see from Fig. 4, the STTC-based EXIT plane spans from the horizontal line $[I_E(\text{MLC}) = \{0 \rightarrow 3\}, I_{E1}(\text{TCM}) = 0, I_E(\text{STTC}) = 2.0148]$ to the horizontal line $[\text{I}_\text{E}(\text{MLC}) = \{0 \rightarrow 3\}, I_{E1}(\text{TCM}) = 4, I_E(\text{STTC}) = 2.3493]$. Since the STTC decoder was unable to converge to the $I_E(\text{STTC}) = 4$ position, a two-stage concatenated scheme based on STTC, such as for example the STTC-NSC benchmark scheme, would fail to reach an error free performance at $E_b/N_0 = -0.5$ dB. However, as we can see from Figs. 4 and 5, the TCM decoder's output trajectories converged to the $[I_E(\text{MLC}) = 3, I_{E1}(\text{TCM}) = 4]$ and $[I_E(\text{MLC}) = 3, I_{E2}(\text{TCM}) = 3]$ positions, respectively. This indicates that an error-free performance can be attained by the three-stage concatenated STTC-TCM-2RSC scheme at $E_b/N_0 = -0.5$ dB, despite employing a poorly converging STTC scheme. As we can observe from Fig. 5, the intersection of the EXIT planes includes the vertical line at $[I_E(\text{MLC}) = 3, I_{E2}(\text{TCM}) = 3, I_E(\text{STTC}) = \{1.9 \rightarrow 4\}]$, hence the recursive TCM decoder has in fact aided the non-recursive STTC decoder in achieving a possible early convergence at $I_E(\text{STTC}) = 1.9$, rather than only at $I_E(\text{STTC}) = 4$, when the STTC-TCM scheme is iteratively exchanging extrinsic information with the MLC decoder. This indicates that when a non-recursive STTC is employed, a three-stage concatenated coding scheme is necessary for approaching the MIMO channel's capacity. Better constituent codes may be designed for the three-stage concatenated coding scheme based on the 3-D EXIT chart of Fig. 5. More explicitly, good constituent codes would result in two EXIT planes that intersect at as low an I_E(STTC) value in Fig. 5, as possible. It should be noted however that such schemes may require a high number of iterations, because they may operate between the cut-off rate and the capacity, which typically imposes a high delay and high complexity.

Figure 6 shows that convergence can be achieved at a low SNR value of $E_b/N_0 = -0.77$ dB, when a longer interleaver block length of 100 000 16 QAM symbols is employed. By

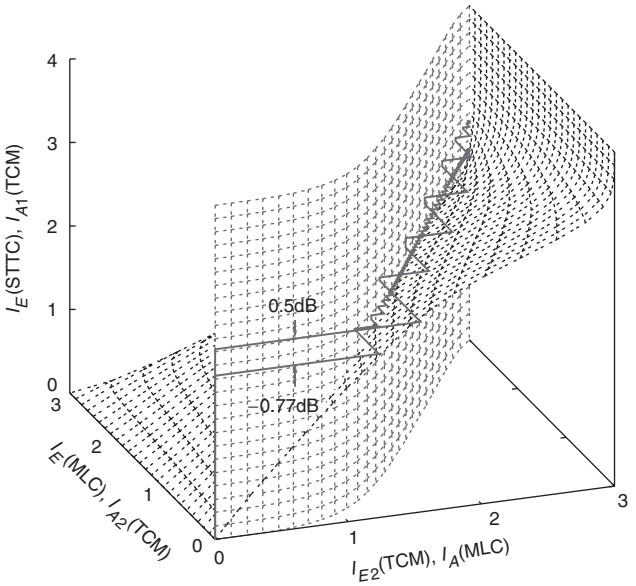

Fig. 6 *The 3-D EXIT chart and the iteration trajectory between the TCM and MLC decoders at $E_b/N_0 = -0.77$ dB, when a block length of 100 000 16QAM symbols is used, and at $E_b/N_0 = 0.5$ dB, when a block length of 1160 16QAM symbols is used*
The EXIT plane spanning from the vertical line $[I_E(\text{MLC}) = 0, I_A(\text{MLC}) = 0, I_E(\text{STTC}) = \{0 \rightarrow 4\}]$ to the vertical line $[I_E(\text{MLC}) = 3, I_A(\text{MLC}) = 3, I_E(\text{STTC}) = \{0 \rightarrow 4\}]$ was computed based on the MLC decoder's output $P_e^3(c)$ and the other EXIT plane was computed based on the TCM decoder's output $P_i^2(u)$

contrast, convergence is only achieved at a higher SNR value of $E_b/N_0 = 0.5$ dB, when a shorter interleaver block length of 1160 16 QAM symbols is used. Hence, the lower-delay STTC-TCM-2RSC scheme of Section 2 employing an interleaver length of 1160 16 QAM symbols is approximately 2.3 dB away from the STTC channel capacity of −1.80 dB and 0.99 dB from the STBC channel capacity of −0.49 dB at a throughput of 1.98 BPS, according to Fig. 3. When a longer interleaver delay of 100 000 16 QAM symbols can be tolerated, the effective throughput becomes approximately 2.00 BPS, since the code rate loss owing to termination symbols/bits has been reduced slightly. In this case, the STTC-TCM-2RSC scheme which converged at $E_b/N_0 = -0.77$ dB is only about 1 dB away from the STTC channel capacity of −1.77 dB and it performs 0.32 dB better than the STBC channel capacity of −0.45 dB at a throughput of 2.00 BPS.

5 Simulation results

We continue our discourse by characterising the attainable performance of the proposed MPEG-4 based video telephone schemes using both the bit error ratio (BER) and the average video peak signal-to-noise ratio (PSNR) [26].

Figures 7 and 8 depict the class-1 and class-2 BER against E_b/N_0 performance of the 16 QAM-based STTC-TCM-2NSC and STTC-TCM-2RSC schemes, respectively, when communicating over uncorrelated Rayleigh fading channels. Specifically, the class-1 bits benefit from more than an order of magnitude lower BER at a given SNR, than the class-2 bits. Figure 9 compares the overall BER performance of the STTC-TCM-2NSC and STTC-TCM-2RSC schemes. More explicitly, the STTC-TCM-2RSC scheme is outperformed by the STTC-TCM-2NSC arrangement, when the number of iterations is lower than eight. At BER $= 10^{-4}$ an approximately 4 dB and 6 dB iteration gain was attained by the STTC-TCM-2NSC and STTC-TCM-2RSC schemes, respectively, when the number of iterations was increased from one to eight. Note in Figs. 8 and 9 that the STTC-TCM-2RSC scheme suffers from an error floor, despite having a high iteration gain, which is due to the employment of RSC outer codes instead of the NSC outer codes.

The BER performance curves of STTC-BICM-2RSC and STTC-NSC are shown in Fig. 10. Note that if we

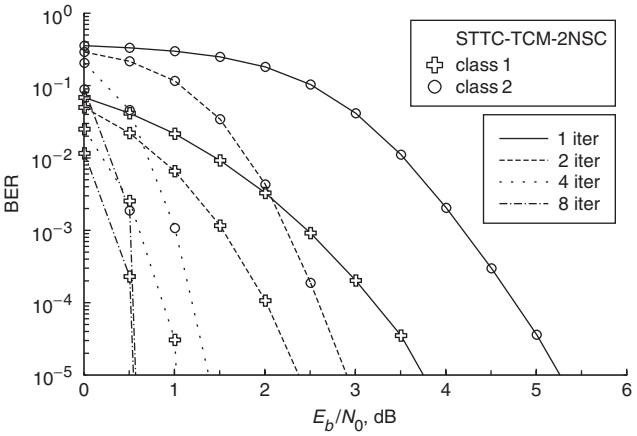

Fig. 7 *BER against E_b/N_0 performance of the 16QAM-based STTC-TCM-2NSC assisted MPEG-4 scheme, when communicating over uncorrelated Rayleigh fading channels*
The effective throughput was **1.98 BPS**

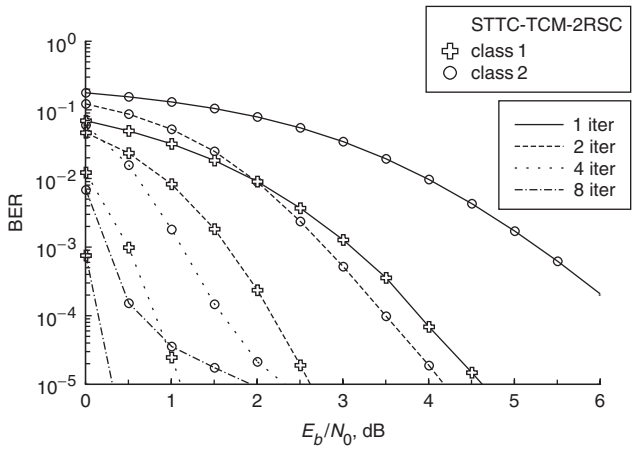

Fig. 8 *BER against E_b/N_0 performance of the 16QAM-based STTC-TCM-2RSC assisted MPEG-4 scheme, when communicating over uncorrelated Rayleigh fading channels*
The effective throughput was **1.98 BPS**

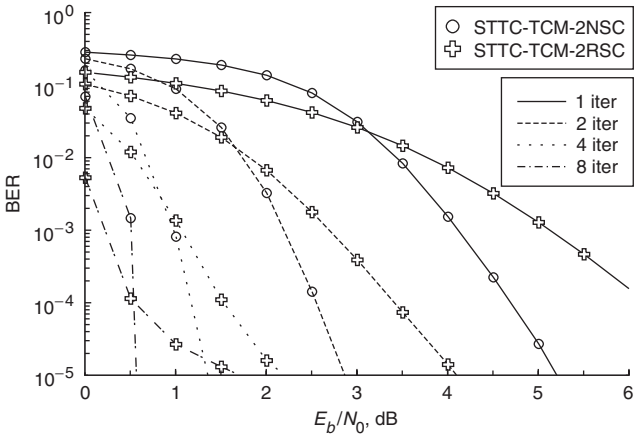

Fig. 9 *BER against E_b/N_0 performance of the 16QAM-based STTC-TCM-2NSC and STTC-TCM-2RSC assisted MPEG-4 schemes, when communicating over uncorrelated Rayleigh fading channels*
The effective throughput was **1.98 BPS**

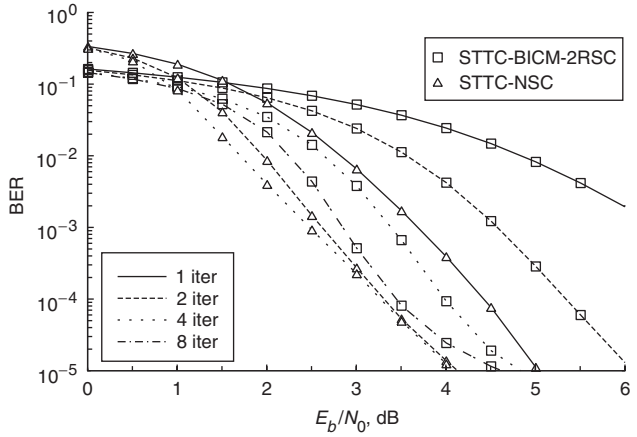

Fig. 10 *BER against E_b/N_0 performance of the 16QAM-based STTC-BICM-2RSC and STTC-NSC assisted MPEG-4 schemes, when communicating over uncorrelated Rayleigh fading channels*
The effective throughput of STTC-BICM-2RSC and STTC-NSC was **1.98 BPS** and **1.99 BPS**, respectively

reduce the code memory of the NSC constituent code of the STTC-NSC benchmark scheme from $L_0 = 6$ to 3, the best possible performance becomes poorer. If we increased L_0 from 6 to 7 (or higher), the decoding complexity would be significantly increased, while the attainable best possible performance is only marginally improved. Hence, the STTC-NSC scheme having $L_0 = 6$ constitutes a powerful benchmark scheme in terms of its performance against complexity trade-offs. As observed in Fig. 10, the performance of the STTC-BICM-2RSC scheme is even worse than that of the STTC-NSC benchmark scheme. More explicitly, STTC-BICM-2RSC employing eight iterations cannot outperform the STTC-NSC arrangement employing two iterations. By changing the outer code to NSC, i.e. using the STTC-BICM-2NSC scheme, the attainable performance cannot be further improved. The complexity of the STTC-TCM-2NSC/2RSC arrangement having four (or eight) iterations corresponds to 160 (or 320) trellis states, which is similar to that of the STTC-NSC scheme having two (or four) iterations. Hence, at a complexity of 160 (or 320) trellis states, the E_b/N_0 performance of the STTC-TCM-2NSC (or STTC-TCM-2RSC) scheme is approximately 2 dB (or 2.8 dB) better than that of the STTC-NSC benchmark scheme at BER $= 10^{-4}$.

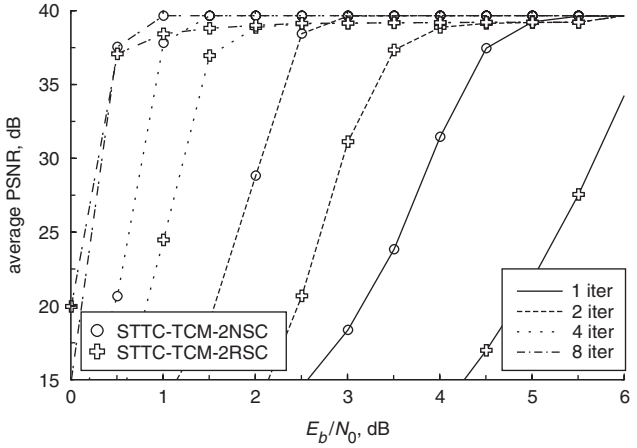

Fig. 11 *Average PSNR against E_b/N_0 performance of the proposed 16QAM-based STTC-TCM-2NSC and STTC-TCM-2RSC assisted MPEG-4 schemes, when communicating over uncorrelated Rayleigh fading channels*
The effective throughput was **1.98 BPS**

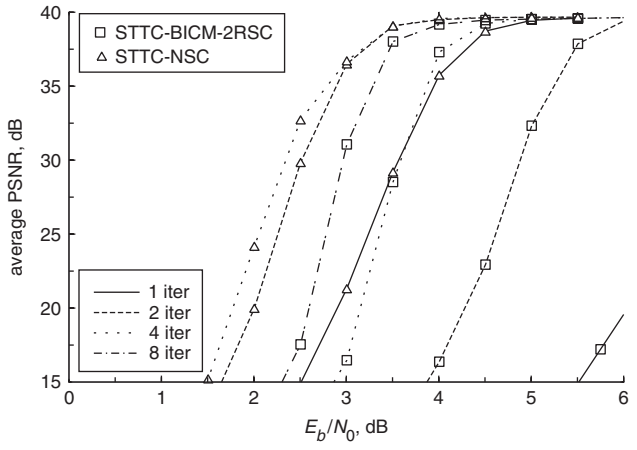

Fig. 12 *Average PSNR against E_b/N_0 performance of the 16QAM-based STTC-BICM-2RSC and STTC-NSC assisted MPEG-4 benchmark schemes, when communicating over uncorrelated Rayleigh fading channels*
The effective throughput of STTC-BICM-2RSC and STTC-NSC was **1.98 BPS** and **1.99 BPS**, respectively

Let us now consider the PSNR against E_b/N_0 performance of the systems characterised in Figs. 11 and 12. The PSNR performance trends are similar to our observations made in the context of the achievable BER results. The maximum attainable PSNR is 39.7 dB. Observe in Fig. 11 that the BER floor of the STTC-TCM-2RSC scheme resulted in a slightly lower maximum attainable PSNR value, when we had $E_b/N_0 < 6$ dB. Furthermore, when employing eight iterations at $E_b/N_0 = 0.5$ dB, the PSNR of STTC-TCM- 2RSC was found to be slightly lower than that of the STTC-TCM-2NSC arrangement, although the BER of STTC-TCM-2RSC is significantly lower than that of the STTC-TCM-2NSC scheme, as it is evidenced in Fig. 9. This is because STTC-TCM-2RSC suffers from a higher transmission frame error ratio, despite having a lower BER, in comparison to the STTC-TCM-2NSC scheme at $E_b/N_0 = 0.5$ dB.

6 Conclusions

In conclusion, a jointly optimised source-coding, outer channel-coding, inner coded modulation and spatial diversity aided turbo transceiver was studied and proposed for MPEG-4 wireless video telephony. With the aid of an MLC scheme that consists of two different-rate NSCs/RSCs the video bits were unequally protected according to their sensitivity. The employment of TCM improved the bandwidth efficiency of the system and by utilising STTC spatial diversity was attained. The performance of the proposed STTC-TCM-2NSC/STTC-TCM-2RSC scheme was enhanced with the advent of an efficient iterative decoding structure exchanging extrinsic information across three consecutive blocks. Explicitly, it was shown in Section 4 that when a non-recursive STTC decoder is employed, a three-stage concatenated iterative decoding scheme is required for approaching the MIMO channel's capacity. It was shown in Figs. 9 and 11 that the STTC-TCM-2RSC scheme required $E_b/N_0 = 0.5$ dB in order to attain BER $= 10^{-4}$ and PSNR > 37 dB, which is 2.3 dB away from the corresponding MIMO channel's capacity. However, if the proposed STTC-TCM-2RSC scheme is used for broadcasting MPEG-4 encoded video, where a longer delay can be tolerated, the required E_b/N_0 value is only 1 dB away from the MIMO channel's capacity, as evidenced by comparing Figs. 3 and 6.

7 Acknowledgments

The financial support of both the EPSRC, Swindon UK and the EU under the auspices of the Phoenix project is gratefully acknowledged. Furthermore, the authors would like to express their thanks to Dr. J. Kliewer for his mathematical insight contributing towards the creation of the EXIT chart software used.

8 References

1 Ungerboeck, G.: 'Channel coding with multilevel/phase signals', *IEEE Trans. Info. Theory*, 1982, **IT-28**, pp. 55–67
2 Hanzo, L., Liew, T.H., and Yeap, B.L.: 'Turbo coding, turbo equalisation and space time coding for transmission over wireless channels' (John Wiley IEEE Press, New York, USA, 2002)
3 Zehavi, E.: '8-PSK trellis codes for a Rayleigh fading channel', *IEEE Trans. Commun.*, 1992, **40**, pp. 873–883
4 Tarokh, V., Seshadri, N., and Calderbank, A.R.: 'Space-time codes for high rate wireless communication: performance analysis and code construction', *IEEE Trans. Inf. Theory*, 1998, **44**, pp. 744–765

5 Tao, M., and Cheng, R.S.: 'Diagonal block space-time code design for diversity and coding advantage over flat Rayleigh fading channels', *IEEE Trans. Signal Process.*, 2004, **52**, (4), pp. 1012–1029
6 Ng, S.X., Guo, F., and Hanzo, L.: 'Iterative detection of diagonal block space time trellis codes, TCM and reversible variable length codes for transmission over Rayleigh fading channels'. IEEE Vehicular Technology Conf., Los Angeles, USA, 26–29 September 2004
7 Wachsmann, U., Fischer, R.F.H., and Huber, J.B.: 'Multilevel codes: theoretical concepts and practical design rules', *IEEE Trans. Inf. Theory*, 1999, **45**, pp. 1361–1391
8 Morelos-Zaragoza, R.H., Fossorier, M.P.C., Shu, L., and Imai, H.: 'Multilevel coded modulation for unequal error protection and multistage decoding– part I: symmetric constellations', *IEEE Trans. Commun.*, 2000, **48**, pp. 204–213
9 Lin, S., and Constello, Jr. D.: 'Error control coding: fundamentals and applications' (Prentice-Hall, Englewood Cliffs, NJ, 1982)
10 ISO/IEC JTC1/SC29/WG11, 'Information technology – generic coding of audio-visual objects', in *'Part 2: Visual. Draft ISO/IEC 14496-2 (MPEG-4)', version 1, ISO/IEC*, (Geneva), 1998
11 ISO/IEC JTC1/SC29/WG11 W2502 in *ISO/IEC 14496-2. Final Draft International Standard. Part 2: Visual*, (Atlantic City), 1998
12 Kliewer, J., Ng, S.X., Hanzo, L.: 'Efficient computation of EXIT functions for non-binary iterative decoding', Submitted to the *IEEE Transactions on Communications*, 2005
13 Foschini, Jr. G.J.: 'Layered space-time architecture for wireless communication in a fading environment when using multi-element antennas', *Bell Labs Tech. J.*, 1996, **1**, (2), pp. 41–59
14 Hanzo, L., Ng, S.X., Webb, W., and Keller, T.: 'Quadrature amplitude modulation: from basics to adaptive trellis-coded, turbo-equalised and space-time coded OFDM, CDMA and MC-CDMA systems' (John Wiley and Sons, New York, USA, 2000)
15 Proakis, J.: 'Digital communications' (McGraw-Hill, New York, 1987)
16 Gallager, R.: 'Information theory and reliable communication' (John Wiley and Sons, 1968)
17 Telatar, E.: 'Capacity of multi-antenna Gaussian channels', *Euro. Trans. Telecommun.*, 1999, **10**, pp. 585–595
18 Vucetic, B., and Yuan, J.: 'Space-time coding' (John Wiley-IEEE Press, New York, USA, 2003)
19 Alamouti, S.M.: 'A simple transmit diversity technique for wireless communications', *IEEE J. Sel. Areas Commun.*, 1998, **16**, pp. 1451–1458
20 Tarokh, V., Jafarkhani, H., and Calderbank, A.: 'Space-time block codes from orthogonal designs', *IEEE Trans. Inf. Theory*, 1999, **45**, pp. 1456–1467
21 Ng, S.X., and Hanzo, L.: 'Space-time IQ-interleaved TCM and TTCM for AWGN and Rayleigh fading channels', *Electron. Lett.*, 2002, **38**, pp. 1553–1555
22 ten Brink, S.: 'Convergence behaviour of iteratively decoded parallel concatenated codes', *IEEE Trans. Commun.*, 2001, **49**, pp. 1727–1737
23 Chen, H., and Haimovich, A.: 'EXIT charts for turbo trellis-coded modulation', *IEEE Commun. Lett.*, 2004, **8**, pp. 668–670
24 Grant, A.: 'Convergence of non-binary iterative decoding'. Proc. of the IEEE Global Telecommunications Conf. (GLOBECOM), San Antonio TX, USA, November 2001, pp. 1058–1062
25 Tüchler, M.: 'Convergence prediction for iterative decoding of threefold concatenated systems'. Proceedings of the IEEE Global Telecommunications Conf. (Globecom'02), Taipei, Taiwan, 17–21 November 2002, Vol. 2, pp. 1358–1362
26 Hanzo, L., Cherriman, P.J., and Street, J.: 'Wireless video communications: second to third generation systems and beyond' (IEEE Press, NJ, USA, 2001)